Numerical Evaluation of High Order Finite Element Time Domain Formulations in Electromagnetics

Neilen Marais and David B. Davidson

Abstract

This paper compares three full-wave Finite Element Time Domain (FETD) formulations. The first is based on the vector wave equation; the others on Maxwell's equations, viz. the EBHD formulation that discretises $\vec{E}$, $\vec{B}$, $\vec{H}$ and $\vec{D}$ and the EB formulation that discretises only $\vec{E}$ and $\vec{B}$. The latter two formulations use a combination of 1-form and 2-form discretisation to avoid an auxiliary mesh. A novel method for making the EBHD formulation operational is presented. Conditions for Finite Difference Time Domain (FDTD)-like explicit operation are discussed. The formulations are compared numerically by solving a three dimensional cavity and a rectangular waveguide using high order field representations up to mixed 4th order. The error balance between time integration and field representation is investigated. Difficulties in making the EBHD formulation operational which have not previously been addressed in the literature are discussed and worked around. Novel numerical results show that the EBHD formulation has serious performance limitations.

Index Terms

Finite element methods, Electromagnetic transient analysis, high-order methods, numerical analysis

I. INTRODUCTION

For solving the transient response of electromagnetic systems, finite element time domain (FETD) methods using unstructured meshes are suitable for complex geometries; the structured meshes used by standard finite difference time domain (FDTD) methods limit the achievable accuracy on such geometries. Most FETD methods require matrix solution at each time-step while FDTD is fully explicit; barring errors in geometric modelling FDTD will usually be more computationally efficient than FETD.

Department of Electrical and Electronic Engineering University of Stellenbosch, South Africa nmarais@gmail.com, davidson@sun.ac.za

Vector full-wave Finite Element Time Domain (FETD) methods commonly fall into two categories; those based on the vector wave equation (VWE), and those based on the coupled Maxwell's equations. To date wave equation formulations have been the most popular, and are well described in the engineering literature, e.g. [1]. This may partly be due to the simplicity of implementing it in basic form given an existing frequency domain FEM code.

Three formulations based on the coupled Maxwell's equations that do not call for auxiliary meshes have been proposed. One based on discretising the $\vec{E}$ and $\vec{H}$ fields as well as the $\vec{D}$ and $\vec{B}$ flux densities is presented in [2] and expanded upon in [3]. The others discretise only $\vec{E}$ and $\vec{B}$. One approach uses discrete 2-form elements for $\vec{B}$ [4], [5] while another [6] uses a discontinuous element-wise polynomial representation. Below, the first formulation is labeled the EBHD formulation and the other two are collectively labeled as EB formulations. The complementarity features of 1- and 2- Whitney forms [7] obviates a complementary mesh.

Using Newmark-β time integration [2] the VWE formulation can be unconditionally stable, a great advantage when meshes with varying element sizes are desired. The Maxwell's formulations involve only first order time derivatives, simplifying the implementation of PML mesh termination and dispersive material modelling [8]. The EBHD formulation is claimed to support explicit FDTD style operation, while the EB formulation is simpler than the EBHD formulation.

The main contributions of this paper are: a comparison of the popular VWE formulation and two coupled Maxwell's formulations, presentation of a novel well-defined method to make the EBHD formulation operational and a critical evaluation of the EBHD formulation's accuracy. All the formulations are implemented with field representation ranging from mixed 1st to mixed 4th order. The error balance between time integration and field representation as the order of field representation increases is investigated. Some of the tradeoffs involved in the choice of explicit or unconditionally stable implicit time integration schemes are also discussed.

II. FORMULATION

Full-wave FEM formulations are generally used to solve Maxwell's equations in a domain Ω:

$$\nabla \times \vec{E} = -\mu \frac{\partial \vec{H}}{\partial t} = -\frac{\partial \vec{B}}{\partial t} \tag{1}$$

$$\nabla \times \vec{H} = \vec{J} + \epsilon \frac{\partial \vec{E}}{\partial t} = \vec{J} + \frac{\partial \vec{D}}{\partial t}, \tag{2}$$

where $\vec{J}$ is the impressed source current.

Eliminating $\vec{H}$ from (1) and (2), the Helmholtz vector wave equation is obtained:

$$\nabla \times \frac{1}{\mu} \nabla \times \vec{E} + \epsilon \frac{\partial^2 \vec{E}}{\partial t^2} = -\frac{\partial \vec{J}}{\partial t}. \tag{3}$$

Zero initial values and boundary conditions are specified, making (1), (2) or (3) well posed initial value problems. For simplicity, Dirichlet boundary conditions are considered here. More sophisticated boundary conditions may be used depending on the nature of the problem being solved, see e.g. [1].

A. Field Discretisation

Using the language of Differential Forms [9], $\vec{E}$ and $\vec{H}$ field quantities are represented as discrete 1-forms (curl-conforming) and $\vec{D}$ and $\vec{B}$ flux densities as discrete 2-forms (div-conforming). Suitable function spaces for their definition are presented in [4]. The concrete hierarchical basis functions of arbitrary order for tetrahedrons defined in [10] and [11] are used for respectively 1-form and 2-form discretisation.

Throughout this paper the notation $\vec{w^{(1)}}$ and $\vec{w^{(2)}}$ will be used for respectively 1-form and 2-form basis functions. E.g. $\vec{w_{ei}^{(1)}}$ and $\vec{w_{bj}^{(2)}}$ respectively refer to the ith 1-form basis function used to discretise an $\vec{E}$ field and the jth 2-form basis function used to discretise a $\vec{B}$ flux density. The degrees of freedom (DOFs) are represented as column vectors, respectively $\{e\}$ and $\{b\}$.

The curl of 1-forms is a subset of 2-forms. A discrete 2-form can exactly represent the curl of a 1-form. With mixed 1st order discrete 1-form $\vec{A}$ and discrete 2-form $\vec{B}$ on the same mesh, $\vec{B} = \nabla \times \vec{A}$ has the discrete equivalent $\{b\} = [C_a]\{a\}$; $[C_a]$ is a highly sparse circulation matrix that depends only on mesh topology with 1 or -1 entries [5], [12]. This property is maintained when using hierarchical higher order discretisations where the solenoidal 2-form basis functions are defined as the curl of the rotational 1-form basis functions.

A full 2-form discretisation spans both solenoidal and non-solenoidal function spaces. However the $\vec{B}$ and in source free regions $\vec{D}$ flux densities are solenoidal. The hierarchical 2-form basis functions defined in [11] are split into solenoidal and non-solenoidal sets. The non-solenoidal basis function DOFs will be identically zero as they are only updated by the curls of the fields. The non-solenoidal basis functions can simply be omitted from the fluxes, reducing the number of DOFs needed.

B. Vector Wave Equation (VWE) Formulation

The vector wave equation formulation is well known and is discussed in detail in [1, §12]. Time integration is performed using the Newmark-β method [13], [14]. With $\beta \geq \frac{1}{4}$ this method is

unconditionally stable. For a detailed discussion of stability see [15]. Assuming homogeneous Dirichlet boundary conditions, the fully discrete update equation is

$$
\begin{aligned}
\left[[M_\epsilon] + \Delta t^2 \beta [S_\mu]\right]\{e\}^{n+1} \quad = \quad & \\
& \left[2[M_\epsilon] - \Delta t^2(1-2\beta)[S_\mu]\right]\{e\}^n \\
& - \left[[M_\epsilon] + \Delta t^2 \beta [S_\mu]\right]\{e\}^{n-1} \\
& - \Delta t^2 \left[\beta\{f\}^{n+1} + (1-2\beta)\{f\}^n + \beta\{f\}^{n-1}\right], \quad (4)
\end{aligned}
$$

where $[M_\epsilon]$ and $[S_\mu]$ are the square mass and stiffness matrices with entries

$$
M_{\epsilon_{ij}} = \int_\Omega \epsilon \vec{w}_{ei}^{(1)} \cdot \vec{w}_{ej}^{(1)} d\Omega \tag{5}
$$

$$
S_{\mu_{ij}} = \int_\Omega \frac{1}{\mu}(\nabla \times \vec{w}_{ei}^{(1)}) \cdot (\nabla \times \vec{w}_{ej}^{(1)}) d\Omega, \tag{6}
$$

$\{e\}$ the vector of $\vec{E}$ field DOFs and $\{f\}$ the current driving vector.

C. EBHD Maxwell's Formulation

For this scheme, the Maxwell's equations (1), (2) are used to implement a leapfrog scheme [3]. The fields $\vec{E}$, $\vec{H}$ are discretised as 1-forms and the flux densities $\vec{D}$, $\vec{B}$ as 2-forms. Writing time as $t = n\Delta t$ where n is the integer time-step and Δt is the constant time step size, we have $\vec{E}(n)$ and $\vec{D}(n)$ and half a time step apart $\vec{H}(n+\frac{1}{2})$ and $\vec{B}(n+\frac{1}{2})$. Starting with known fields and fluxes at $t = n\Delta t$,

$$
\{b\}^{n+\frac{1}{2}} = \{b\}^{n-\frac{1}{2}} - \Delta t[C_e]\{e\}^n \tag{7}
$$

$$
\{h\}^{n+\frac{1}{2}} = [\star_b]\{b\}^{n+\frac{1}{2}} \tag{8}
$$

$$
\{d\}^{n+1} = \{d\}^n + \Delta t[C_h]\{h\}^{n+\frac{1}{2}} - \{j\}^{n+\frac{1}{2}} \tag{9}
$$

$$
\{e\}^{n+1} = [\star_d]\{d\}^{n+1}. \tag{10}
$$

The $[\star_b]$ and $[\star_d]$ matrices are respectively the magnetic and electric discrete Hodge star operators. The Hodge operator here transforms a 2-form representation into an equivalent 1-form representation [9], also applying he constitutive relations, i.e. $\vec{H} = \frac{1}{\mu}\vec{B}$ and $\vec{E} = \frac{1}{\epsilon}\vec{D}$.

In [3] an explicit collocation-based Hodge operator is outlined, but it requires the integration of the undefined tangential component of 2-form basis functions at inter-element boundaries. A novel Hodge operator is constructed by a projection process where both sides of (8) are tested using the $\{w_h^{(1)}\}$ basis functions, resulting in

$$
[M_h]\{h\}^{n+\frac{1}{2}} = [P_{\mu h}]\{b\}^{n+\frac{1}{2}} \tag{11}
$$

giving

$$[\star_b] = [M_h]^{-1}[P_{\mu h}]. \tag{12}$$

Here $[M_h]$ is the $\{w_h^{(1)}\}$ unit-material mass matrix, and $[P_{\mu h}]$ the projection of $\{w_b^{(2)}\}$ onto $\{w_h^{(1)}\}$. The matrix entries are

$$M_{h_{ij}} = \int_\Omega \vec{w}_{hi}^{(1)} \cdot \vec{w}_{hj}^{(1)} d\Omega \tag{13}$$

$$P_{\mu h_{ij}} = \int_\Omega \frac{1}{\mu} \vec{w}_{hi}^{(1)} \cdot \vec{w}_{bj}^{(2)} d\Omega. \tag{14}$$

This operator is well defined since it involves only volume integrals. A discrete Hodge operator for (10) is derived similarly.

The projection Hodge is not explicit since the $[M_h]$ and $[M_e]$ mass matrices have to be inverted. In light of the EBHD formulation's poor performance using the projection Hodge (see Section III-C), attempts at making the collocation-based explicit Hodge operational were not pursued as its performance can be expected to be even poorer.

D. EB Maxwell's Formulation

This formulation, also based on (1), (2), discretises $\vec{E}$ as a 1-form and $\vec{B}$ as a 2-form and was first outlined in [4], with practical results in [5]. Because the $\vec{E}$ discretisation is curl-conforming (1) is trivially verified in discrete form:

$$\frac{d}{dt}\{b\} = -[C_e]\{e\}. \tag{15}$$

More care is needed for (2). First re-write it as

$$\epsilon \frac{\partial \vec{E}}{\partial t} = \nabla \times (\frac{1}{\mu}\vec{B}) - \vec{J}. \tag{16}$$

Now a Galerkin procedure is applied by testing both sides of (16) with $\{\vec{w}_e^{(1)}\}$. A Green's identity is used to transfer the curl of $\vec{B}$ to the testing functions since the 2-form discretisation is not curl-conforming. The discrete counterpart to (16), assuming Dirichlet boundary conditions, is

$$[M_\epsilon]\frac{d}{dt}\{e\} = [P_\mu]\{b\} - \{f\}. \tag{17}$$

$[M_\epsilon]$ is the $\{w_e^{(1)}\}$ mass matrix defined in (5), $[P_\mu]$ the projection of $\{w_b^{(2)}\}$ onto $\nabla \times \{w_e^{(1)}\}$ and $\{f\}$ is the projection of $\vec{J}$ onto $\{w_e^{(1)}\}$. The $[P_\mu]$ and $\{f\}$ entries are:

$$P_{\mu_{ij}} = \int_\Omega \frac{1}{\mu}(\nabla \times \vec{w}_{ei}^{(1)}) \cdot \vec{w}_{bj}^{(2)} d\Omega, \tag{18}$$

$$f_i = \int_\Omega \vec{J} \cdot \vec{w}_{ei}^{(1)} d\Omega. \tag{19}$$

While not pursued in this paper, the discontinuous element-wise constant $\vec{B}$ discretisation used in [6] is also capable of representing exactly the curl of the low order $\vec{E}$ discretisation, and would yield numerically identical results. Such a $\vec{B}$ discretisation would require 3 DOFs per element, although the notation in [6] seems to imply only one. In a tetrahedral mesh each element contributes on average two unique face DOFs, leading to a lower DOF count if a mixed first order discrete 2-form is used.

$\vec{E}$ and $\vec{B}$ are discretised half a time-step apart as in Section II-C. Starting with known $\vec{E}$ and $\vec{B}$ at $t = n\Delta t$, the update equations are

$$\{b\}^{n+\frac{1}{2}} = \{b\}^{n-\frac{1}{2}} - \Delta t [C_e]\{e\}^n \tag{20}$$

$$\{e\}^{n+1} = \{e\}^n + [M_\epsilon]^{-1}\Delta t([P_\mu]\{b\}^{n+\frac{1}{2}} \tag{21}$$

$$- \{f\}^{n+\frac{1}{2}}).$$

E. Explicit Operation

Explicit operation of these formulations requires explicit time integration *and* field discretisation that results in a diagonal mass matrix. The leapfrog time integration used by the EBHD and EB formulations is explicit, as is the Newmark-β with $\beta = 0$. Explicit time integration will at best result in conditional stability; suitable implicit schemes, such as Newmark-β with $\beta \geq \frac{1}{4}$ are unconditionally stable.

Δt must be smaller than a certain value for leap-frog time-integration to be stable. The largest stable time-step [16] is

$$\Delta t_{\max} = \frac{2}{\sqrt{\psi_{\max}}}, \tag{22}$$

where $\psi_{\max}$ is the largest eigenvalue of the semi-discrete system as described in Sec. III-D. This is essentially a generalisation of the Courant limit familiar from FDTD methods to general meshes. Raising the field representation order p on a given mesh will increase $\psi_{\max}$, leading to a smaller $\Delta t_{\max}$.

With mixed 1st order rectangular brick elements the mass matrix can be diagonalised by using trapezoidal geometric integration. Using the EB formulation, or the VWE formulation with $\beta = 0$, the classic Yee FDTD is recovered [5], [17]. Gauss point mass lumping [18] can be applied to higher order rectangular elements. A generalised mass lumping scheme [19] significantly increases the mass-matrix sparsity of general hexahedral elements. Mass lumping for tetrahedral elements up to second order has been developed [20], but no general method for diagonalising higher order tetrahedrons or other non-Cartesian shaped 1-form elements are available in the literature. With a non-diagonal mass matrix, the VWE with explicit time integration ($\beta = 0$) results in a better conditioned matrix equation

than the implicit ($\beta \geq 0$) case, since the singular $[S_\mu]$ matrix is excluded from the LHS of (4); this is similar to the LHS that results from using leap-frog integration with the EB and EBHD formulations.

III. CAVITY RESONANCE PROBLEM

To evaluate the basic operation and convergence of FEM formulation a simple problem that depends on no other aspects of the method is required. The resonance of a rectangular PEC cavity is such a problem; it has well known resonant modes and the analytical solution is straightforward and can be found in many engineering electromagnetics texts. If a cavity is fed with a wide band pulse designed to excite all the modes, resonant peaks should appear at the modes' cutoff frequencies. The measured frequency-locations of the resonant peaks do not depend on the nature of the numerical excitation or measurement; the only requirement is that the source excites all the modes of interest.

Frequency domain FEM methods have an error term due to the geometric modelling of the chosen element and another due to the field truncation within the element. When discretising a geometry that the elements can conform to, such as the rectangular cavity under consideration here, only the field truncation error remains. Time domain FEM also introduces an error term due time integration. By solving the semi-discrete system as an eigen-problem as described in Sec. III-D the effect of time integration can be isolated.

A. Problem Configuration

A 29x23x19 m cavity (as analysed in [21]) is discretised using tetrahedrons with a nominal edge length of 3 m. Note that in this and the following sections the speed of light is normalized to 1 m/s. This cavity has evenly spaced mode cutoff frequencies over an approximately 2:1 bandwidth starting from the lowest mode cutoff frequency. The source and measurement points were chosen to excite and capture the response of all the modes over this bandwidth. The cavity is excited by a $(1; 1; 1)$ directed electric dipole at $r_s = (7, 2, 4)$ using a sine-wave modulated by a Gaussian pulse time-waveform. The waveform is designed with a centre frequency (F_c) of 0.0375 Hz and 90% of F_c -6 dB bandwidth. The E-field response at $r_m = (17, 14, 12)$ is recorded at each time-step. The frequency response is analysed between the frequencies $f_{min} = 0.025$ Hz and $f_{max} = 0.050$ Hz.

B. Result Extraction

In general FFT analysis Δt is chosen such that $f_{\text{nyq}} = 2f_{max}$ where f_{nyq} is the Nyquist frequency and no significant spectral content exists for $f > f_{max}$, yielding $\Delta t_{\text{nyq}} = \frac{1}{2f_{max}}$. Here, Δt is bound by

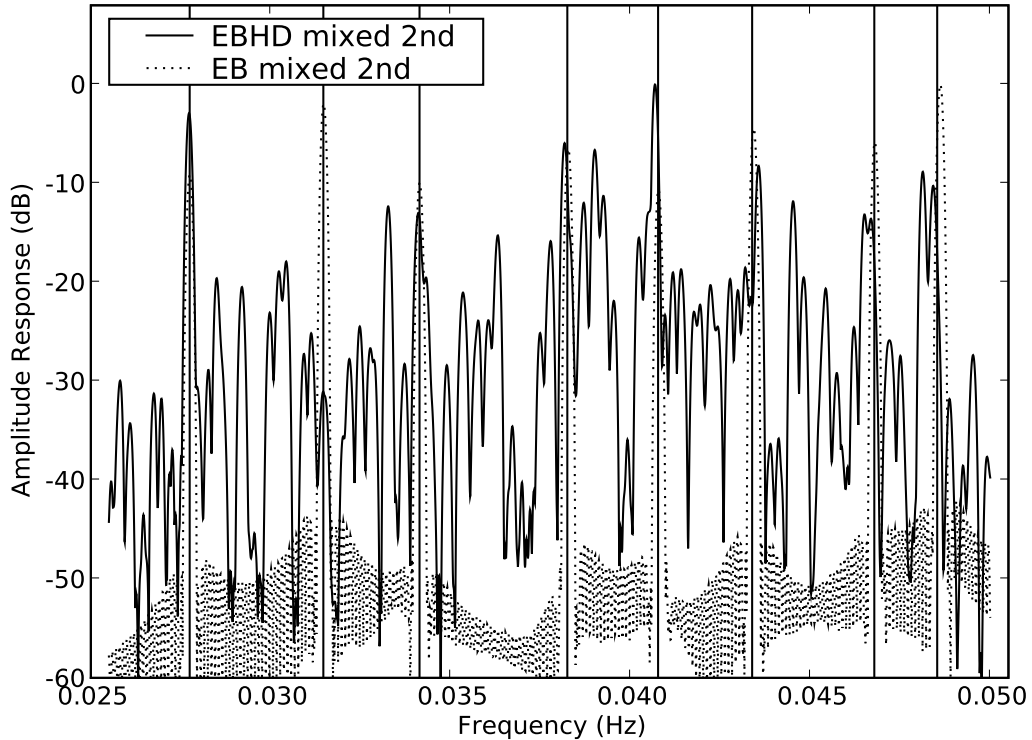Fig. 1. FFT of time domain cavity response using mixed 2nd order elements and $\Delta t = \frac{1}{64}$. Vertical bars indicate the analytically calculated cavity mode cutoff frequencies. The EB result shows clear peaks at the cutoff frequencies while the EBHD result shows spurious peaks throughout the frequency range.

time integration accuracy and, for the conditionally stable schemes, stability criteria. The resulting Δt is usually much smaller than required by the Nyquist criterion.

Maintaining sufficient frequency resolution leads to unpractically large FFTs as Δt is reduced. By choosing Δt as an integral divisor of Δt_{nyq}, i.e. $\Delta t = \Delta t_{\mathrm{nyq}}/n$ and using every nth simulation time sample, the FFT size is constant in Δt. Choosing $\Delta t_{\mathrm{nyq}} = 4$ sets f_{nyq} high enough to avoiding frequency aliasing.

The three $\vec{E}$-field component time series are each weighted with a Hamming window and zero extended. To provide sufficient frequency resolution, the cavity systems were time stepped for 40 000 s.

To find the resonant peaks the absolute value of the three $\vec{E}$-field FFTs are added and a simple peak finding algorithm was applied. Sample responses can be seen in Figs. 1 and 2. A single result datum is finally obtained by calculating the frequency-normalised RMS error of the 8 frequencies under
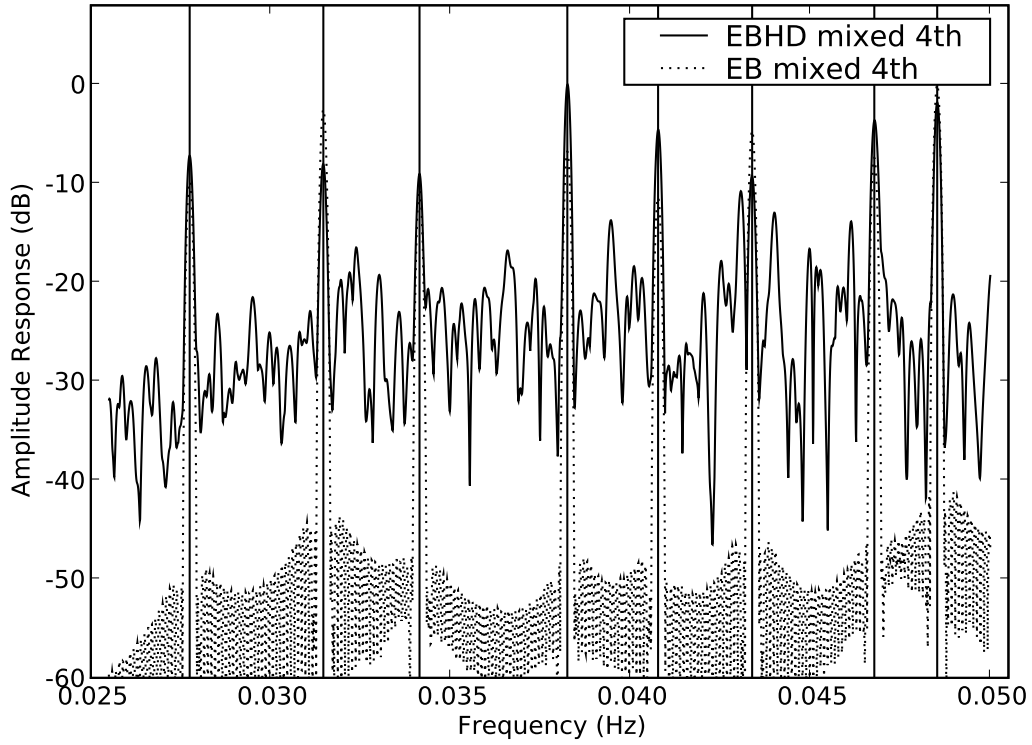
Fig. 2. FFT of time domain cavity response using mixed 4th order elements and $\Delta t = \frac{1}{64}$. Vertical bars indicate the analytically calculated cavity mode cutoff frequencies. In contrast to the mixed 2nd order case, the EBHD result shows recognisable peaks at the cutoff frequencies while the spurious peaks have reduced amplitude.

consideration.

C. Cavity Resonance Results

Error convergence in element basis order for different time-step sizes using the VWE formulation and unconditionally stable Newmark-β time integration is shown in Fig. 3. The ability to use arbitrarily large time-steps is useful when illustrating the separate convergence in Δt and p. The result labeled "eigen" represents perfect time integration and was calculated as described in Sec. III-D. For sufficiently small values of Δt the error is dominated by the field error, showing p convergence as for the eigen result.

Fig. 4 shows convergence in Δt for various basis orders. Generated from the same raw data as Fig. 3, it represents a dual interpretation. Even at the largest Δt considered the mixed 1st order error is clearly dominated by the field truncation error. Using 3rd order basis functions $O(\Delta t^2)$ convergence is seen for
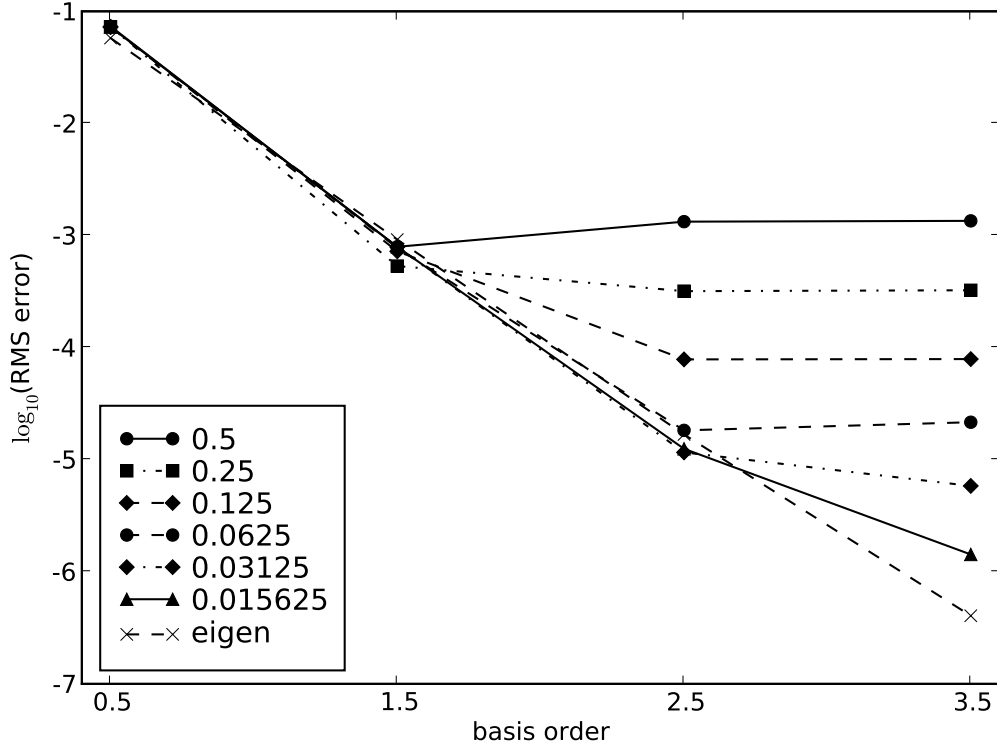
Fig. 3. Convergence in field-basis order using unconditionally stable Newmark-β time integration. Legend shows values of Δt, or "eigen" for the semi-discrete system's eigenvalues.

all but the smallest values of Δt where field truncation error contributes significantly, while the error using 4th order basis functions is dominated by time integration throughout. The corresponding results using the EB formulation is shown in Fig. 5. The major difference between the Newmark-based and EB formulations are the result of conditional stability for the latter, resulting in the omission of larger Δt values for the higher basis-order runs. Within the Δt and basis-order parameter space common to both formulations the results are similar with the EB formulation being slightly more accurate in general. For some specific combinations of Δt and basis order, most easily visible for $\Delta t = 0.25$ s and mixed 2nd order basis functions, the field and time integration errors appear to cancel partly when using Newmark-β, resulting in a more accurate determination of resonant frequencies than the eigen solution provides; this behaviour was not observed in the EB solutions. At the EB stability limit the total error is dominated by the time integration error but the field truncation error already contributes significantly; refinement in Δt reduces the error but at a rate less than $O(\Delta t^2)$.
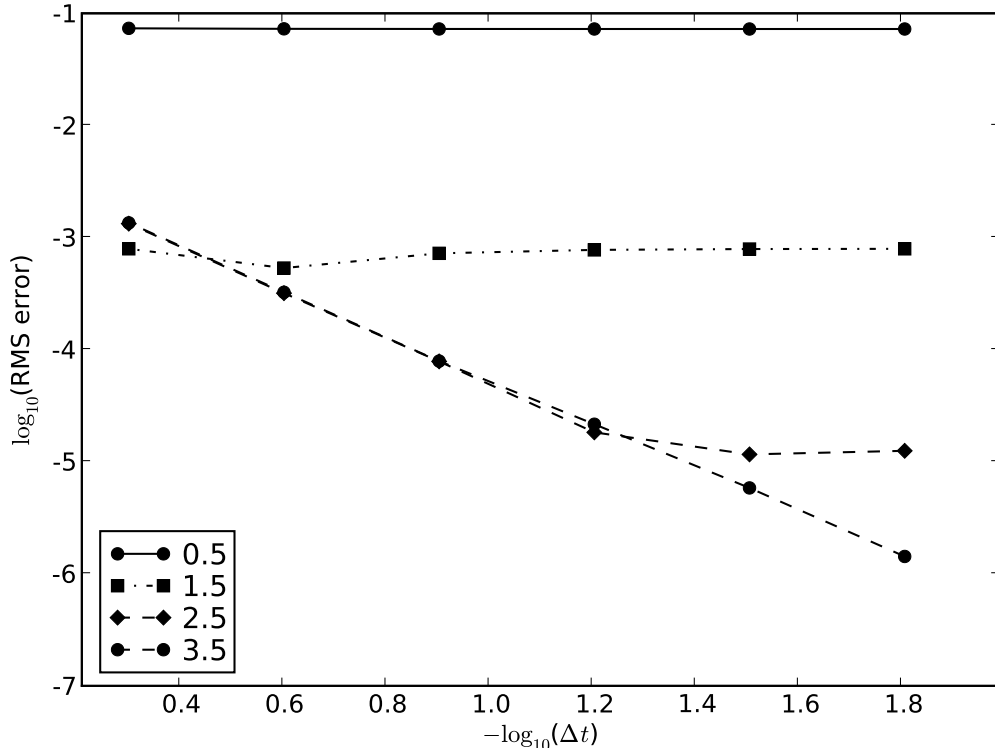
Fig. 4. Convergence in Δt using unconditionally stable Newmark-β time integration. Legend shows field-basis order.

It was not possible to automatically extract resonant frequencies from the EBHD results due to the prevalence of spurious modes as can be seen in Fig. 1 and Fig. 2. The mixed 4th order results in Fig. 2 do show some more strongly exited modes that correspond to the correct modal resonant frequencies. Manually excluding the spurious modes, the mixed 4th order EBHD solution shows an RMS error of 0.01 percent over the resonant mode frequencies. The corresponding mixed 2nd, 3rd and 4th order EB results are 0.068, 0.0014 and 7×10^{-5} percent respectively. This shows that the mixed 4th order EBHD accuracy is of the same order of magnitude as the mixed 2nd order EB solution while requiring about twice the computational work of the 4th order EB solution. The correspondence of the apparently correct mode resonances calculated by the EBHD formulation to physical modes is investigated in Sec. III-D.

At the smallest Δt, the systems were stepped 5.12×10^6 times. No traces of late time instability was noted for either EB or EBHD methods. The VWE showed slow linear growth [22]. The growth was positively correlated to element order, but never significantly affected the results for this problem.
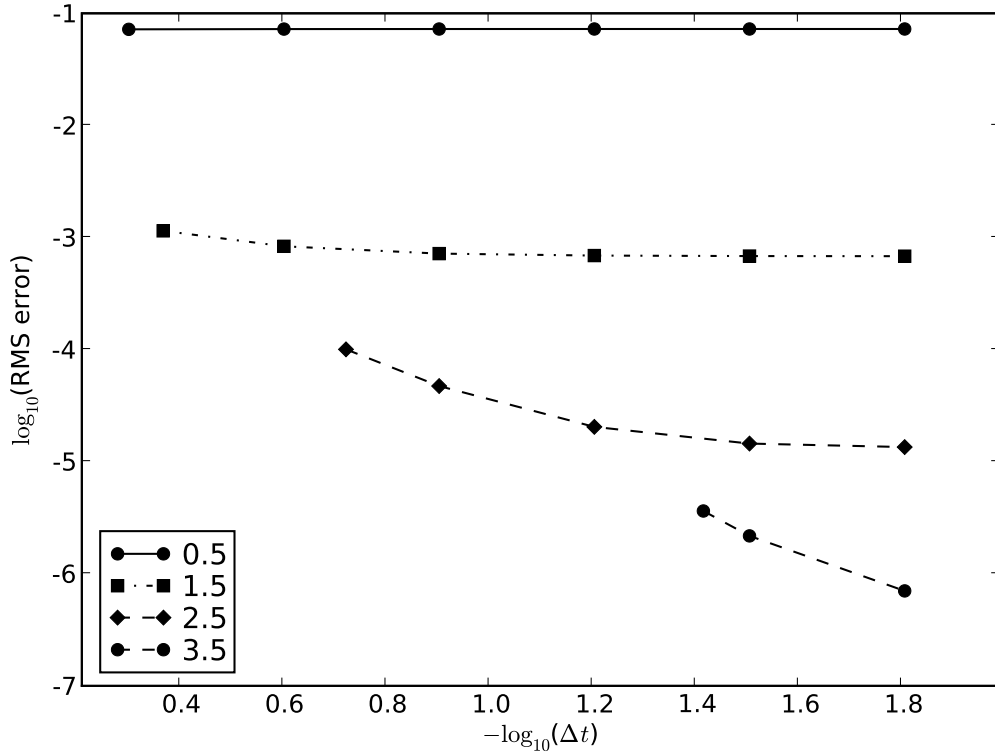
Fig. 5. Convergence in Δt using the EB formulation and conditionally stable leap-frog time integration. Legend shows field-basis order. Larger Δt values not calculated for high basis-order due to stability requirements.

D. Cavity Eigen Solution

The source-free semi-discrete forms of the formulations are transformed to the frequency domain by replacing $\frac{d}{dt}$ by $-j\omega$ and all the field/flux unknowns except for $\vec{E}$ are eliminated. The remaining equation can be cast in the standard form of a generalised eigen-problem. Solving this eigen-problem on a cavity yields the cavity mode cutoff wavenumbers as eigenvalues. Replacing $\frac{d}{dt}$ by $-j\omega$ implies perfect time integration, hence any error in the eigen solution is determined solely by errors in geometric field interpolation.

The VWE formulation yields the well known eigen system,

$$[S_\mu]\{e\} = \omega^2[M_\epsilon]\{e\}. \tag{23}$$

Using the Galerkin discrete Hodge operator for the EBHD formulation, the eigen system is

$$[P_{\epsilon e}][C_h][M_h]^{-1}[P_{\mu h}][C_e]\{e\} = \omega^2[M_e]\{e\}. \tag{24}$$

For the EB formulation it is

$$[P_\mu][C_e]\{e\} = \omega^2[M_\epsilon]\{e\}. \tag{25}$$

The respective eigen systems were solved using the same mesh as in Section III. The calculated values of the four lowest cut-off frequencies are shown in Table I.

Formulation	Mode Cutoff Wavenumber				
Analytical	0.174	0.198	0.214	0.240	0.240
VWE.	0.163	0.187	0.212	0.223	0.235
EBHD	0.037	0.057	0.060	0.061	0.067
EB	0.163	0.187	0.212	0.223	0.235

TABLE I

ANALYTIC VS. COMPUTED MODE CUTOFF FREQUENCIES USING MIXED 1ST ORDER ELEMENTS. THE FOUR LOWEST VALUES

LARGER THAN ZERO ARE SHOWN.

Mirroring the time-domain results, the EBHD eigen-spectrum has many spurious modes. These closely spaced spurious modes exist throughout the whole eigen-spectrum. Similar spurious modes persist in the EBHD spectrum when h and/or p adaptation is applied; the other formulations converge at the expected rate [10]. Note that the mesh used is quite coarse, resulting in somewhat inaccurate results with the lowest order elements. The VWE and EB formulations are equivalent for the eigen-problem since they both model exactly the same spaces. Indeed, by noting that $[P_\mu][C_e] = [C_e]^T[M_\mu]^{-1}[C_e]$ it can be shown [23] that $[P_\mu][C_e] = [S_\mu]$.

To see if the seemingly non-spurious EBHD modes represent physical solutions, the corresponding field is reconstructed using the eigenvector and compared to the physical solution. Fig. 6 shows a visual comparison of the field-plots of an x–y cross-section. The non-spurious EBHD mode compares well to the analytical and EB modes. The other EBHD mode shown, which has a cutoff frequency very close to that of the physical mode, shows a clearly non-physical field distribution.

A consistent discrete Hodge should be isomorphic. This implies that if $\vec{E}$ is represented using discrete 1-forms defined on the primary mesh, $\vec{D}$ should be represented by discrete 2-forms defined on the barycentric dual mesh [12], [24], [23], [25]. The number of edges on the primary mesh is equal to the number of faces on the dual mesh, leading to the isomorphism. These properties are implicitly satisfied by the VWE and EB formulations. Attempting to use the primary mesh for all quantities makes an
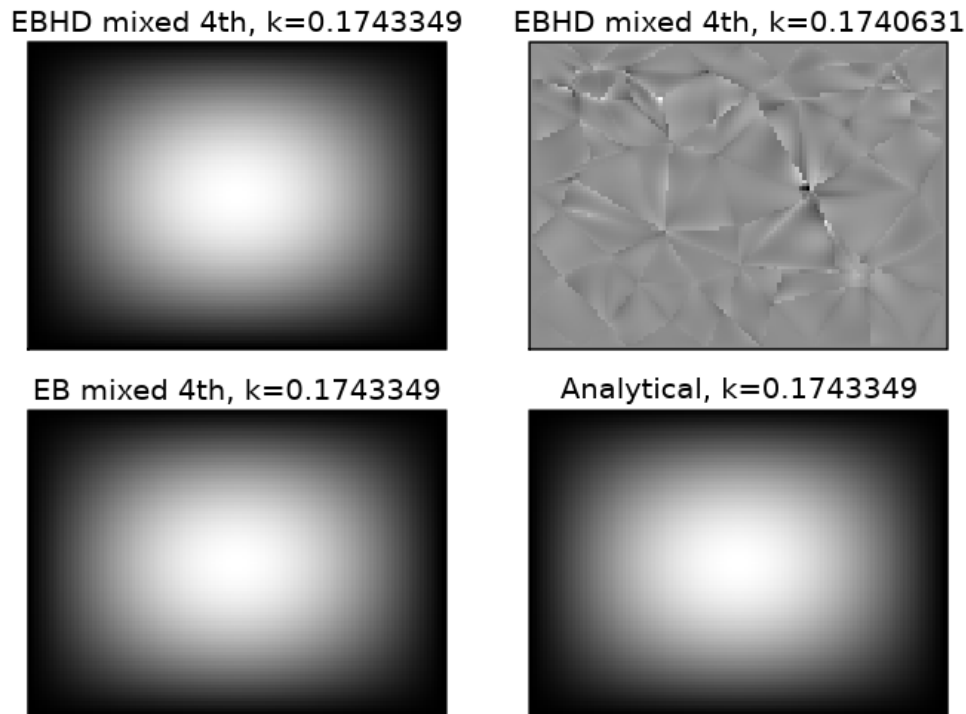
Fig. 6. Magnitude of $\vec{E}_z$ field component of the TE101 mode and a spurious EBHD mode with a cutoff frequency close to that of the real TE101 mode. Calculated over an x-y cross-section at $z = 9.5$ m.

isomorphism between e.g. $\vec{E}$ and $\vec{D}$ impossible, since the number of edges $(\vec{E})$ and faces $(\vec{D})$ on the primary mesh are not equal, resulting in the spurious modes exhibited by the EBHD formulation.

The eigenvalue with the largest magnitude is of interest since it determines the largest stable time-step size that can be used with conditionally stable time integration; larger magnitudes require smaller time-steps. The largest eigenvalue can be determined efficiently using e.g. ARPACK [26]. Using the same mesh and basis function order the EBHD semi-discretisation consistently yields a smaller maximal eigenvalue, hence a larger maximum time-step. For the coupled 1st order case the largest EB eigenvalue is 1.25 vs. 0.39 for the EBHD system. The EBHD value also seems to grow much more slowly as the basis order is increased; mixed 4th order discretisation yields a maximum eigenvalue of 2707 for the EB and only 141 for the EBHD semi-discretisation. While this means that for a given discretisation a larger value of Δt can be used with the EBHD formulation than with EB, the inaccuracy of the EBHD results negate this advantage in practice.

IV. RECTANGULAR WAVEGUIDE TRANSIENT RESPONSE

In contrast to the results in the previous sections, a waveguide calculation has shown seemingly reasonable performance using the EBHD formulation in [27]. In this section the formulations are compared using a similar problem. The aim is to measure the performance of the formulations independent of other sources of error. The elements used can conform exactly to the rectangular geometry, avoiding geometrical error. It is also desirable to avoid the use of mesh truncation schemes as they would introduce another source of error.

A. Problem Configuration

A waveguide with a cross section of 1 by 0.25 m that has a cutoff frequency $f_c = 0.5$ Hz is considered. While the frequency-domain analytical solution of such a waveguide is well known, applying it in the time domain is non-trivial thanks to the dispersive behaviour of such waveguides. One approach would be to time-step the system until the response has decayed to an insignificant level and approximating the Fourier integral using this response. This would require very long run times and also necessitate the use of a mesh truncation schemes, which is undesirable.

By evaluating the inverse Fourier integral of the analytical frequency domain response the time domain response can be found. A closed form expression of the waveguide impulse response is derived in [28]. Closed form results for a waveguide exited by a CW pulse are also given; using numerical integration to perform time convolution the response to arbitrary driving functions can be obtained. The impulse response presents quite a stiff integrand just after the first energy arrives, requiring the use of adaptive quadrature. This integral has to be evaluated at each time point of interest.

The waveguide is exited at $z = 0$ m using a Gaussian pulse modulated sine-wave with a centre frequency of $2.75f_c$ and a 190% -6 dB bandwidth. Since this waveform extends to positive and negative infinity, it is time-shifted such that at turn-on ($t = 0$) the power level is at -60 dB relative to peak. It is turned off at $t = 1.94$ s where it is again at -60 dB.

An analytic reference result is obtained by evaluating the response at regularly spaced time samples from $t = 0$ to $t = 9$ s at $z = 1$ m; the FFT is applied to the resulting time series. The analytical time-step is chosen as $\Delta t_a = 1/16$ s. While this yields a high enough Nyquist frequency to avoid significant frequency aliasing, any remnant aliasing is made immaterial by choosing the FEM time-steps such that

$$\Delta t = \Delta t_a / m \tag{26}$$

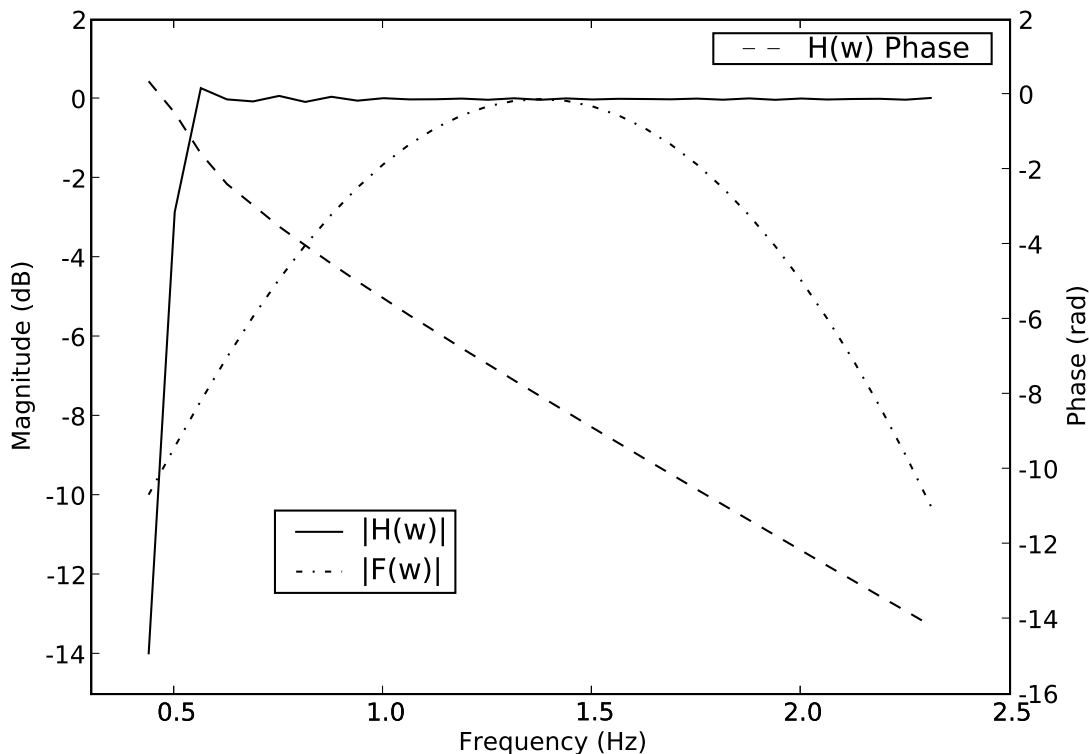and saving only every m'th sample. The FEM results are therefore subject to exactly the same aliasing.

Fig. 7.   FFT of analytically calculated waveguide transient response.

The result is characterised by its discrete transfer function $H(w)$:

$$H(w) = \frac{G(w)}{F(w)} \tag{27}$$

where w is the discrete frequency variable, $G(w)$, the DFT of the output at $z = 1$ m and $F(w)$ the DFT of the driving function. Due to numerical noise, the spectrum of $H(w)$ is only meaningful in the region where $F(w)$ contains considerable energy. The spectrum of $F(w)$ is shown in Fig. 7. Results are considered where $|F(w)|$ is -10 dB relative to peak or larger; the frequency range of interest is 0.4375 Hz to 2.375 Hz.

B. Result Extraction

A short-circuited length of waveguide is meshed using tetrahedrons with a nominal edge length of 0.2 m. Considering the 9 s simulation time, a 5.1 m length of waveguide ensures that no reflections from the short circuited end have time to reach the measurement plane. The TE10 waveguide-mode is excited at

$z = 0$ using an E-field Dirichlet boundary condition matched to the tangential components of the TE10 mode using projection:

$$\int_{\Omega_s} (\hat{n} \times \sum_j e_j \vec{w}_{ej}^{(1)}) \cdot (\hat{n} \times \vec{w}_{ei}^{(1)}) = \int_{\Omega_s} (\hat{n} \times \vec{E}_m) \cdot (\hat{n} \times \vec{w}_{ei}^{(1)}), \tag{28}$$

where $\vec{E}_m$ is the mode-field and Ω_s is the waveguide cross-section. The mesh was constructed with element faces lying in the $z = 1$ m measurement plane. The mode response is extracted at $z = 1$ using the surface integral

$$\tilde{g}(n_{FEM}\Delta t) = \frac{\int_{\Omega_s} (\hat{n} \times \vec{E}_{z=1}) \cdot (\hat{n} \times \vec{E}_m)}{\int_{\Omega_s} (\hat{n} \times \vec{E}_m) \cdot (\hat{n} \times \vec{E}_m)}, \tag{29}$$

where $\vec{E}_{z=1}$ is the numerical field in the plane.

The system is time-stepped for $9/\Delta t$ steps and every m'th value of $g(n_{FEM}\Delta t)$ is stored with m as in (26), yielding a time-series of the same length as the analytical result to which the FFT is applied. The phase and magnitude response of the resulting FFTs are separately compared to the analytical result. A single phase or magnitude datum is obtained by calculating the RMS error over the FFT frequencies from 0.4375 Hz to 2.375 Hz.

C. Rectangular Waveguide Results

Convergence of $|H(w)|$ in basis order is shown in Fig. 8. The error only shows weak dependence on Δt. Since the problem is lossless and conservative time integration is used, the magnitude response of an unobstructed through depends more strongly on the local field truncation error.

Convergence of $\angle H(w)$ is shown in Fig. 9. Phase error is essentially a measure of numerical dispersion. The phase error behaviour shows the same behaviour as seen in Section III-C where $O(\Delta t^2)$ error behaviour is seen until the field truncation error dominates. Solved using the EB formulation, the error behaviour of $|H(w)|$ at the common values of Δt is indistinguishable from the Newmark result. Convergence of $\angle H(w)$ is shown in Fig. 10. With mixed 2nd order and higher field discretisation, the EB results have converged fully in Δt at their respective stability limited values. The mixed 1st order discretisation however shows a larger phase error at the stability limit $\Delta t = 0.0306$ than the Newmark result using $\Delta t = 0.0625$.

It was found that the EBHD result is almost fully converged at the respective stability-limited values of Δt for each basis order. Results for a common value of Δt is shown in Fig. 11. Good convergence is seen in the phase error but only weak convergence in magnitude. It is likely that spurious modes like those seen in Sec. III are being excited, sapping energy out of the TE10 mode. Since the field is integrated
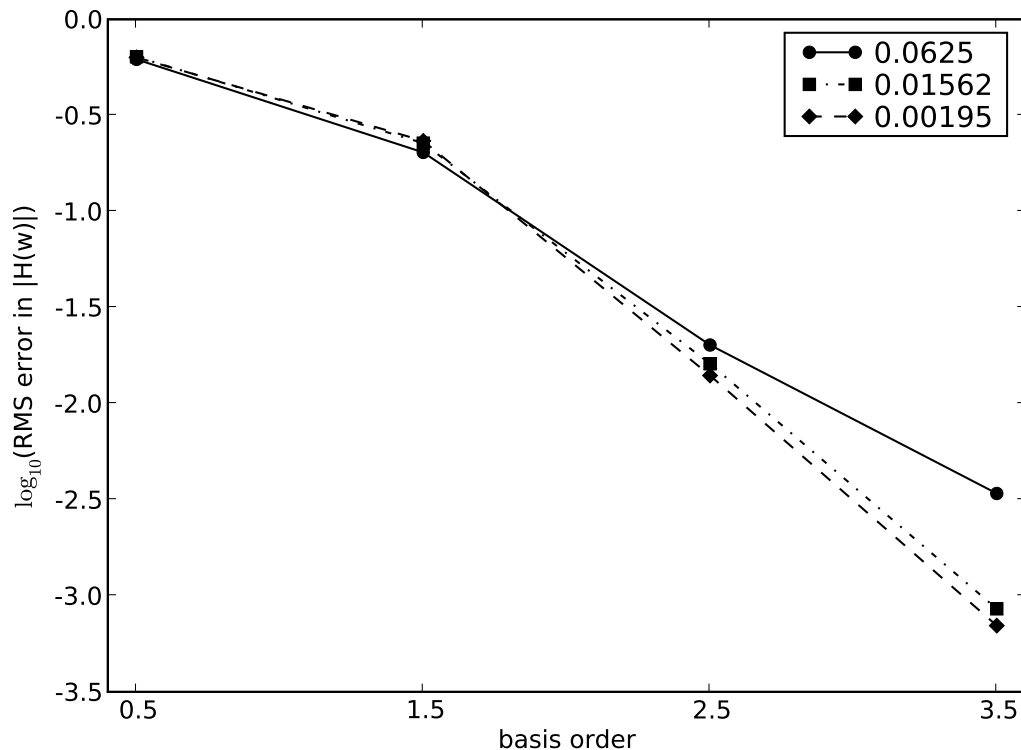
Fig. 8. Convergence of $|H(w)|$ in basis order using unconditionally stable Newmark-β time integration. Legend shows Δt.

over the TE10 mode at the measurement cross-section according to (28), the spurious modes do not affect the received phase as strongly as the energy lost to other modes affect the magnitude accuracy. The effect of the spurious modes is seen more clearly by calculating the field at a point in the center of the $z = 1$ m cross-section; at this point the E_y field component would be identical to the result calculated by (28) for an exact result. As shown in Fig. 12, calculations using the EB formulation show point field and mode integral results that are close, while a significant discrepancy exists in the EBHD calculations. Comparison of the EBHD results to those presented in [27] would have been instructive; unfortunately necessary information such as the time-step size, time waveform and mesh edge length used are not specified in that paper.

V. CONCLUSION

In this paper a summary of three full-wave finite element time domain (FETD) formulations have been presented. The proper discretisation in terms of discrete Whitney forms and the use of hierarchical basis
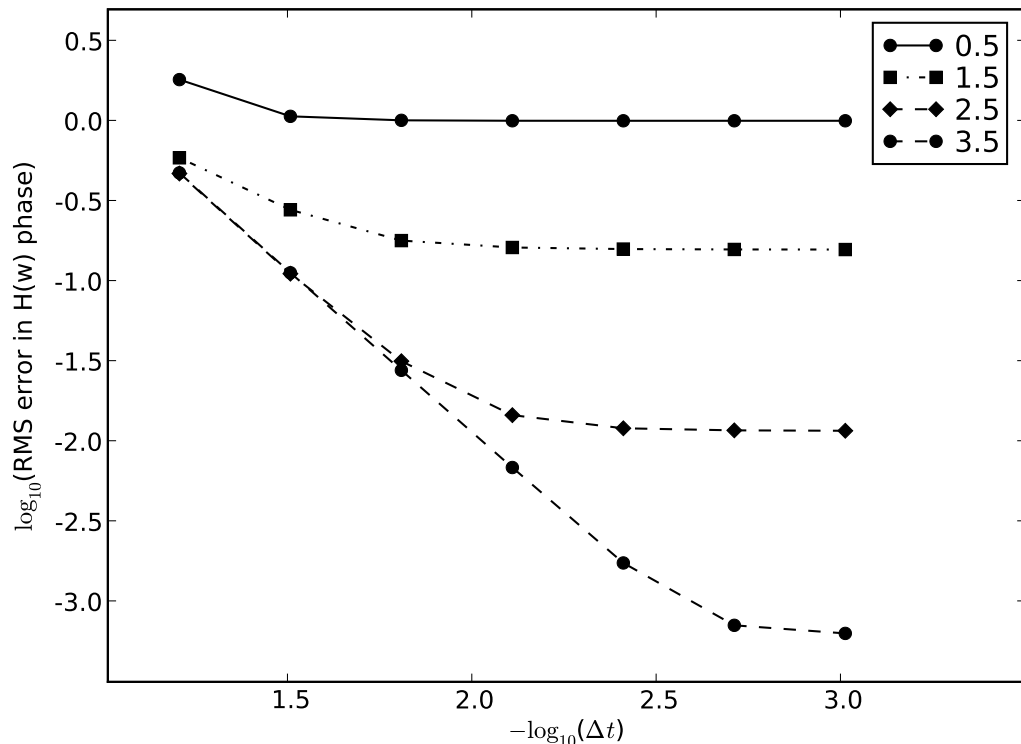
Fig. 9. Convergence of $\angle H(w)$ in Δt using unconditionally stable Newmark-β time integration. Legend shows basis order.

functions to omit redundant 2-form DOFs have been discussed. Unresolved issues regarding the explicit operation of the EBHD as proposed in prior literature have been raised and a novel operational scheme that circumvents the issues, at the cost of solving mass matrices, has been presented.

Novel comparative results using the three presented FETD formulations with high-order field discretisation on canonical EM problems have been presented. The EBHD formulation has been shown to suffer from poor performance due to the presence of spurious modes in its semi-discrete form, making it unsuitable for solving even simple driven problems. The main practical differences between the EB and VWE formulations using respectively leap-frog and unconditionally stable Newmark-β time integration schemes are down to stability considerations.

The EB formulation requires increasing smaller time-steps to remain stable as the order of field-discretisation is increased. Regardless of stability requirements, both the EB and VWE formulations require similarly small time-steps to achieve the accuracy attainable by high-order field modelling. The implicit VWE formulation is seen to be slightly more accurate with low order discretisation and large
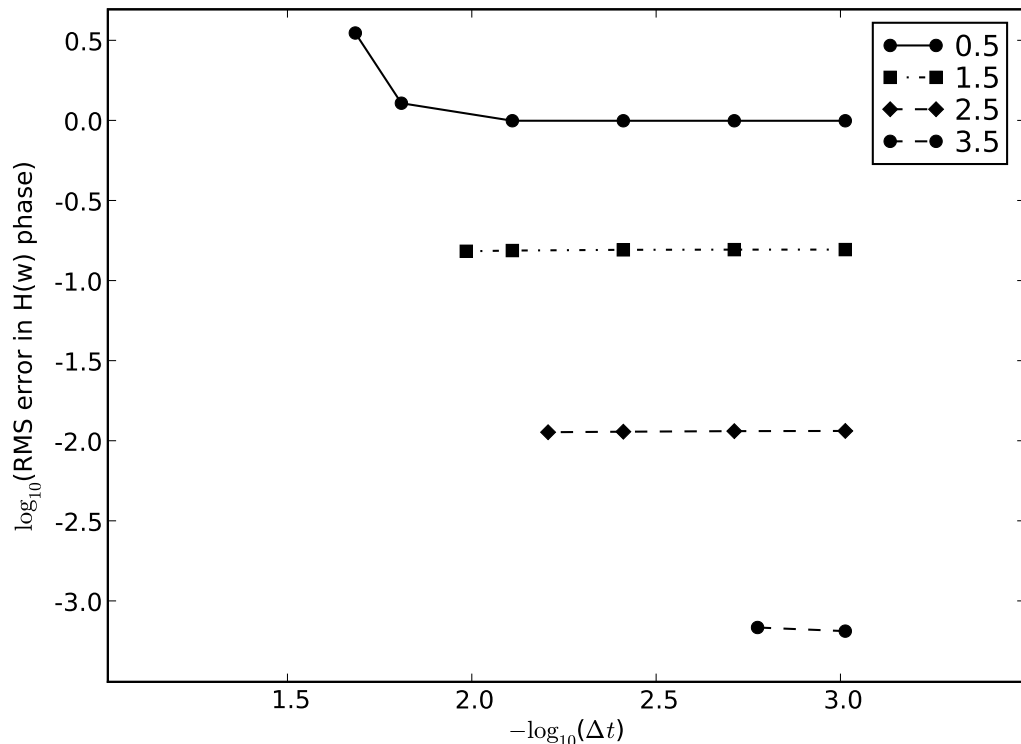
Fig. 10. Convergence of $\angle H(w)$ in Δt using the EB formulation and conditionally stable leap-frog time integration. Legend shows basis order. Larger Δt values not calculated for high basis-order due to stability requirements.

time-steps, whereas the EB formulation has a slight advantage towards the other extreme.

For the EB formulation only mass matrices need to be solved, yielding a better conditioned matrix equation and hence faster iterative solution than the implicit VWE formulation, or explicit operation for elements that have diagonalisable mass. Further, due to the presence of only first order time derivatives, the implementation of PML for domain truncation is much simpler than for the VWE formulation.

These results suggest future work in hybridising the implicit and explicit formulations with suitable diagonalisable elements in a high-order analog to the FDTD-FETD hybrid presented in [17].
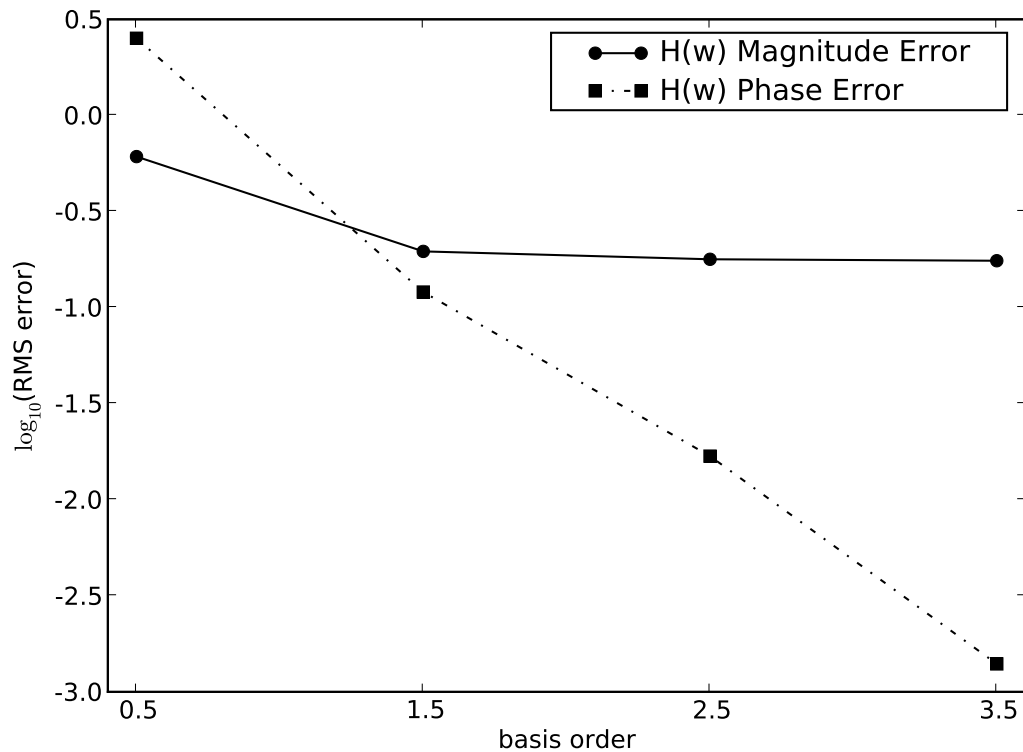
A. Acknowledgements

Fig. 11. Convergence of $|H(w)|$ and $\angle H(w)$ in basis order using the EBHD formulation, conditionally stable leap-frog time integration and $\Delta t = 0.0039$.

REFERENCES

[1] J. Jin, *The Finite Element Method in Electromagnetics*, 2nd ed. John Wiley and Sons, 2002.

[2] J.-F. Lee and Z. Sacks, "Whitney elements time domain (WETD) methods," *IEEE Trans. Magn.*, vol. 31, no. 3, pp. 1325–1329, May 1995.

[3] J.-F. Lee, R. Lee, and A. Cangellaris, "Time-domain finite-element methods," *IEEE Trans. Antennas Propagat.*, vol. 45, no. 3, pp. 430–442, Mar. 1997.

[4] J. C. Nedelec, "Mixed finite elements in $\Re^3$," *Numerische Mathematik*, vol. 35, pp. 315–341, 1980.

[5] M.-F. Wong, O. Picon, and V. Fouad Hanna, "A finite element method based on Whitney forms to solve Maxwell equations in the time domain," *IEEE Trans. Magn.*, vol. 31, no. 3, pp. 1618–1621, May 1995.

[6] M. Feliziani and F. Maradei, "Hybrid finite element solutions of time dependent Maxwell's curl equations," *IEEE Trans. Magn.*, vol. 31, no. 3, pp. 1330–1335, May 1995.

[7] A. Bossavit, "Whitney forms: a class of finite elements for three-dimensional computations in electromagnetism," *IEE Proceedings*, vol. 135, no. 8, pp. 493–500, nov 1988.
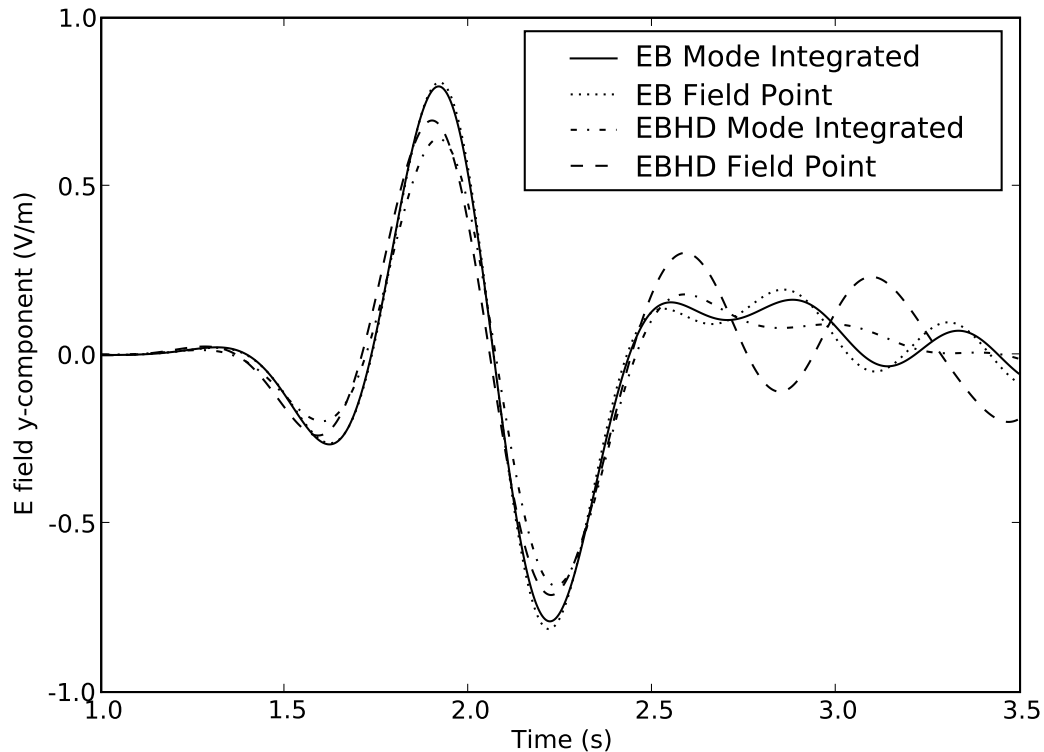
Fig. 12.   Comparison of field-point values at the center of the $z = 1$ m cross-section and mode integrals across the whole section calculated using (28). Results shown calculated using mixed 2nd order basis functions and $\Delta t = 0.0039$.

[8] B. Donderici and F. L. Teixeira, "Mixed finite-element time-domain method for transient Maxwell equations in doubly dispersive media," *IEEE Transactions on Microwave Theory and Techniques*, vol. 56, pp. 113–120, 2008.

[9] G. A. Deschamps, "Electromagnetics and differential forms," *Proc. IEEE*, vol. 69, no. 6, pp. 676–969, June 1981.

[10] J. P. Webb, "Hierarchal vector basis functions of arbitrary order for triangular and tetrahedral finite elements," *IEEE Trans. Antennas Propagat.*, vol. 47, no. 8, pp. 1244–1253, Aug. 1999.

[11] M. M. Botha, "Fully hierarchical divergence-conforming basis functions on tetrahedral cells, with applications," *International Journal for Numerical Methods in Engineering*, vol. 71, pp. 127–148, 2007.

[12] F. L. Teixeira and W. C. Chew, "Lattice electromagnetic theory from a topological viewpoint." *Journal of Mathematical Physics*, vol. 40, p. 169, 1999.

[13] N. M. Newmark, "A method of computation for structural dynamics," *Journal of the Engineering Mechanics Division, American Society of Civil Engineers*, vol. 85, pp. 67–94, July 1959.

[14] O. C. Zienkiewicz, "A new look at the Newmark, Houboult and other time stepping formulas. a weighted residual approach," *Earthquake engineering and structural dynamics*, vol. 5, pp. 413–418, 1977.

[15] T. J. R. Hughes, *Analysis of Transient Algorithms with Particular Reference to Stability Behaviour*, ser. Computational Methods in Mechanics.   Amsterdam: North-Holland, 1983, vol. 1: Computational Methods for Transient Analysis, pp.

67–155, eds. T. Belytschko and T. J. R. Hughes.

[16] G. Rodrigue and D. White, "A vector finite element time-domain method for solving Maxwell's equations on unstructured hexahedral grids," *SIAM Journal of Scientific Computing*, vol. 23, pp. 683–706, 2002.

[17] T. Rylander and A. Bondeson, "Stability of explicit-implicit hybrid time-stepping schemes for Maxwell's equations," *Journal of Computational Physics*, vol. 179, no. 2, pp. 426–438, July 2002.

[18] G. Cohen and P. Monk, "Gauss point mass lumping schemes for Maxwell's equations," *Numerical Methods for Partial Differential Equations*, vol. 14, pp. 63–88, 1998.

[19] A. Fisher, R. N. Rieben, G. H. Rodrigue, and D. A. White, "A generalized mass lumping technique for vector finite-element solutions of the time-dependent Maxwell equations," *IEEE Trans. Antennas Propagat.*, vol. 53, pp. 2900–2910, 2005.

[20] A. Elmkies and P. Joly, "Élments finis d'arête et condensation de masse pour les équations de Maxwell: le cas de dimension 3," *C. R. Acad. Sci. Paris Sér. I Math.*, vol. 325, no. 11, pp. 1217–1222, Dec. 1997.

[21] D. A. White, "Discrete time vector finite element methods for solving Maxwell's equations on 3d unstructured grids," Ph.D. dissertation, Lawrence Livermore National Laboratory, 1997.

[22] R. A. Chilton and R. Lee, "The discrete origin of FETD-Newmark late time instability, and a correction scheme," *Journal of Computational Physics*, vol. 224, pp. 1293–1306, June 2007.

[23] B. He and F. Teixeira, "Geometric finite element discretization of Maxwell equations in primal and dual spaces," *Physics Letters A*, vol. 349, pp. 1–14, 2006.

[24] ——, "On the degrees of freedom of lattice electrodynamics," *Physics Letters A*, vol. 336, pp. 1–7, Feb. 2005.

[25] B. He and F. L. Teixeira, "Differential forms, Galerkin duality, and sparse inverse approximations in finite element solutions of Maxwell equations," *IEEE Transactions on Antennas and Propagation*, vol. 55, pp. 1359–1368, 2007.

[26] R. Lehoucq, D. Sorensen, and C. Yang, *Arpack users' guide: Solution of large scale eigenvalue problems with implicitly restarted Arnoldi methods*, 1997. [Online]. Available: http://citeseer.ist.psu.edu/lehoucq97arpack.html

[27] T. V. Yioultsis, N. V. Kantartzis, C. S. Antonopoulos, and T. D. Tsiboukis, "A fully explicit Whitney element - time domain scheme with higher order vector finite elements for three-dimensional high-frequency problems," *IEEE Trans. Magn.*, vol. 34, no. 5, pp. 3288–3291, Sept. 1998.

[28] S. L. Dvorak, "Exact, closed-form expressions for transient fields in homogeneously filled waveguides," *IEEE Trans. Microwave Theory Tech.*, vol. 42, pp. 2164–2170, 1994.